ELSEVIER

Journal of Nuclear Materials 247 (1997) 21–27

journal of nuclear materials

Laser induced vaporization mass spectrometric studies on UO_2 and graphite

M. Joseph *, N. Sivakumar, D. Darwin Albert Raj, C.K. Mathews

Materials Chemistry Division, Chemical Group, Indira Gandhi Centre for Atomic Research, Kalpakkam 603 102, India

Abstract

A Nd-YAG laser system operated in the Q-switched mode was used to generate vapour plume on UO_2 and graphite targets. The vapour species formed were analysed by a quadrupole mass filter. The time resolved spectrum was obtained for each of the observed vapour species, namely, O, U, UO, UO_2 and UO_3 over UO_2 and C_1 to C_5 over graphite. Time of arrival (TOA) spectra were obtained as a function of laser power density. These TOA data are fitted by the shifted Maxwell Boltzmann distributions so as to obtain the translational temperatures and velocities of the vapour species present in the plume. © 1997 Elsevier Science B.V.

1. Introduction

Estimation of energy release in a hypothetical core disruptive accident of a liquid metal cooled fast breeder reactor (LMFBRs) requires knowledge of vapour pressures of the fuel materials at very high temperatures (up to 5000 K). Conventional experimental techniques such as Knudsen effusion, transpiration, etc. cannot be used at ultra high temperatures (> 3000 K) because of obvious limitations. The need for thermochemical data at these high temperatures and the vapour pressures above the experimental collision-free regime of about 10^{-4} atm is a major driving force for adapting laser heating processes to vaporization studies. If partial pressures of species can be determined under local thermodynamic equilibrium, then thermodynamic functions, activity data can be obtained. Extracting reliable vapour pressure data from laser vaporization mass spectrometry requires detailed understanding of the vaporization process and gas dynamics, which are convoluted in the observable time dependent mass spectrometric signals. In order to quantify the processes occurring when lasers are used to vaporize refractory materials, it is necessary to establish the extent of thermal evaporation, particulate ejection, gas dynamic process, etc.

Ohse et al. suggested the use of a nanosecond wide pulse rather than pulses in the millisecond or microsecond regime, so as to avoid the laser-plume interaction during the vaporization process [1]. Hastie et al. used a 20 ns wide pulse (532 nm) and studied the vaporization behavior of some refractory materials [2]. Earlier, we have studied the vaporization behavior of UO_2 using 8 ns wide (532 nm) laser beam and determined a vapour pressure of 3.8 atm at 4300 K [3]. A linear plot of time-of-arrival (TOA) of these neutral species as a function of the square root of molecular weight indicated the existence of local thermal equilibrium. The surface temperature of UO_2 was determined by an indirect method, by comparing the time of arrival of uranium vapour species over UO_2 with that of the carbon vapour species over graphite. In the present study, time resolved spectra are obtained for the species from UO_2 and graphite as a function laser power density and these spectra are fitted to shifted Maxwell Boltzmann distributions so as to obtain the translational temperatures and velocities of the beam.

2. Experimental facility

A schematic of the experimental apparatus developed for this study is shown in Fig. 1 and the details were reported elsewhere [3]. Briefly, the sample mounted on a kinematic stage was placed in the first chamber. The stage

* Corresponding author. Fax: +91-4114 40 365; e-mail: jay@igcar.ernet.in.

PII S0022-3115(97)00026-3

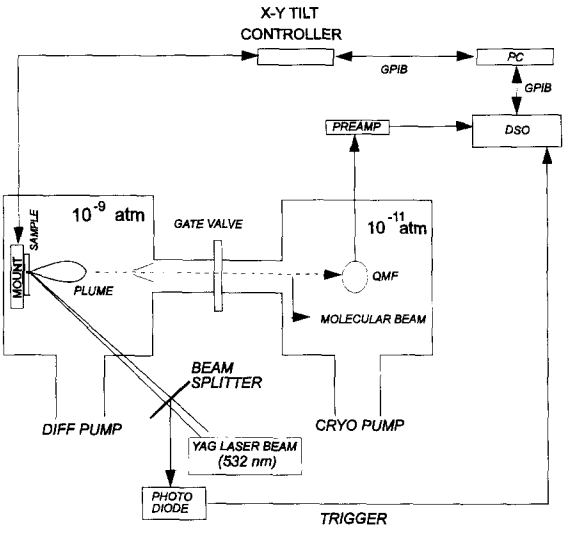

Fig. 1. Schematic of the laser induced vaporization mass spectrometry (LIVMS) facility.

movement was controlled remotely through a personal computer and the sample was rastered. The continuous rastering is required to avoid crater formation, so that reproducible signal is obtained for each laser pulse. In this chamber, the vacuum condition permits the establishment of a high gas expansion pressure ratio and there is minimal perturbation of the vapour plume by post-expansion gas collisions with the background gas molecules. The mass analyzer used was a quadrupole mass filter (QMF) housed in the second chamber in a crossed beam configuration.

A Nd-YAG laser system operated in the Q-switched mode at a repetition rate of 10 Hz (pulse width ≈ 8 ns) with a pulse energy of about 30 mJ at 532 nm was used to generate a reasonably good vapour plume. The power density was varied by changing the distance between the focusing lens and sample surface. Ions formed in the plume were detected with the QMF ionizer-filament turned off, while neutrals were detected by switching on the ionizer and also the deflection plates so as to deflect the ions away from the axis to suppress the ion signal. (The deflection plates were kept about 10 cm from the sample surface.) The analog signal from the channeltron detector through the preamplifier was fed to a digital storage oscilloscope (DSO). In the actual experiment, the mass spectrometer was tuned to the mass of interest and the collection of the signal for about 5 ms from the start of the laser pulse was found to be sufficient to get the time of arrival (TOA) profile of each ion mass. In order to get good signal to noise ratio, the TOA profiles were averaged over 1000 sweeps (for each species). The signal from a photodiode was used to trigger the DSO to start the data collection process. UO_2 samples were of nuclear grade, having a density of 10.6 g/cm^3 and O/U ratio of 2.02, obtained from M/s Nuclear Fuel Complex, Hyderabad, India. The graphite samples are of 99.999% purity and high density (80% of the theoretical density, Grade #DFP-2 of M/s Leico Industries, New York). The samples used were of disc form having ≈ 12 mm diameter and 10 mm thickness.

3. Results and discussion

When the laser power density is increased to above the threshold ($\approx 1 \times 10^7$ W/cm^2) ablation begins, as indicated by the QMF signal. The vapour species observed over UO_2 are O, U, UO, UO_2 and UO_3. In the case of graphite the species detected are C_1 to C_5. Typical TOA profiles obtained for UO and C_3 are shown in Fig. 2. In this study, the laser power density is varied from 3.7×10^7 to 1.5×10^9 W/cm^2. In the case of graphite, ions C_1^+ and C_2^+ are observed, in addition to neutral species when the power density is increased beyond 5×10^8 W/cm^2. But with UO_2, large amount of ions are seen even when the power density is about 1.2×10^8 W/cm^2. This behavior is expected as the effective ionization potential of UO_2 is less than that of graphite [4]. Fig. 3 shows the variation of intensity and TOA of UO as a function of laser power density. At a laser power density of 3.1×10^7 W/cm^2, only neutral species are observed. When the power density is increased to 4.5×10^7 W/cm^2, the neutral/ion ratio is 2.6. On further increasing the power density to 1.2×10^8 W/cm^2 the ion intensity is 6000 times more compared to the signal for the neutral. Moreover, the neutral beam intensity decreases and the TOA increases compared with the power density at 4.5×10^7 W/cm^2. A similar study is carried out on graphite and the results obtained for C_3 species are shown in Fig. 4. The intensity of C_3 increased by a factor of 15 when power density is increased from 4.5×10^7 to 1.2×10^8 W/cm^2 and it increases more modestly (factor of 1.2) for the increase in power density from 1.2×10^8 to 2.6×10^8 W/cm^2. Correspondingly, the TOA also showed a variation by a factor of 1.3 (about 55 μs) in the former region of power densities; the decrease is by a factor of 1.1 (about 15 μs) in the latter region. When the ion intensity increases many fold, the time of arrival increases. The decrease in time of arrival with increase in power density is due to an increase in surface temperature. The increase in time of arrival with many fold increase in ion intensity is due to the space charge field of the ions pulling the neutrals towards the surface. In order to describe the kinetic properties of these laser ablated neutrals and ions, we employed the shifted Maxwell Boltzmann distribution to fit the TOA data. The measured profiles are a convolution of the time response of the detection with the true arrival time distributions. We have deconvoluted the time response of the detection from

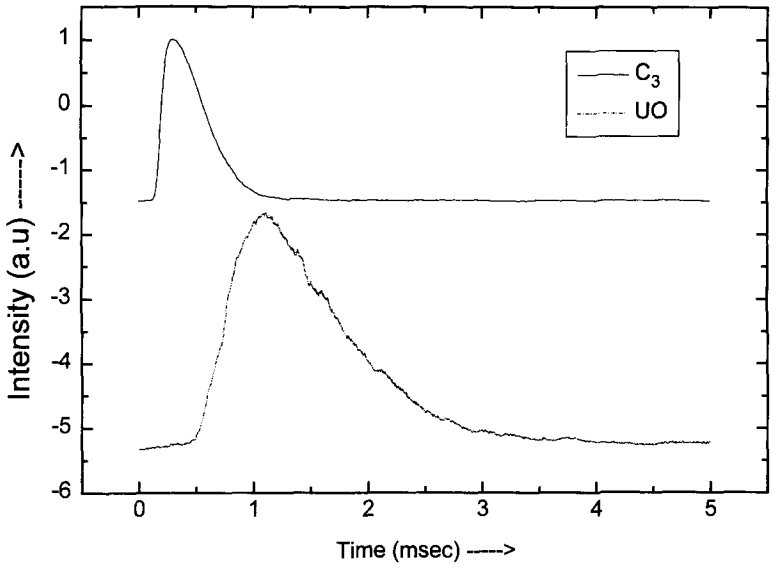

Fig. 2. Typical time-of-arrival (TOA) profiles C_3 and UO species.

the measured profiles following the procedure used by Hastie et al. [5] as

$$J(t) = I^+ + \tau_e \mathrm{d}[I^+(t)]/\mathrm{d}t,$$

where $J(t)$ is the deconvoluted TOA signal, $I^+(t)$ is the time response convoluted signal and τ_e is the time constant. The time constant, 170 μs, was measured by observing the time resolved signal for the ions with a fast preamplifier and then comparing it with the deconvoluted profile of the measured profile obtained with the preamplifier used in this study. The measured profiles and the deconvoluted profiles for different power densities are given in Figs. 5–9 for C_3, UO, C_1^+ and UO^+.

We find that it is possible to fit the deconvoluted profiles to a sum of distributions of the form [6]

$$f(t) = \Sigma A t^{-4} \exp\left(-m\left(\frac{z}{t} - v_{gi}\right)^2 / (2kT_i)\right),$$

where, $f(t)$ is the intensity of the particles arriving at the

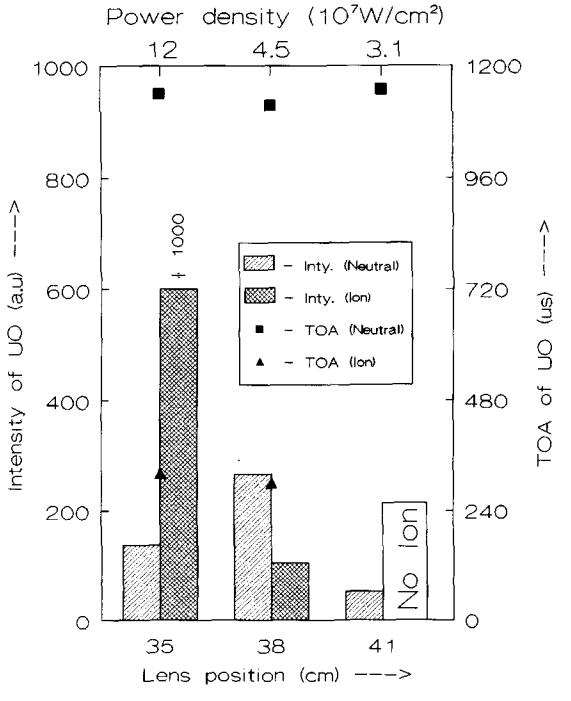

Fig. 3. Intensity and TOA of UO ions and neutrals as a function of laser power density.

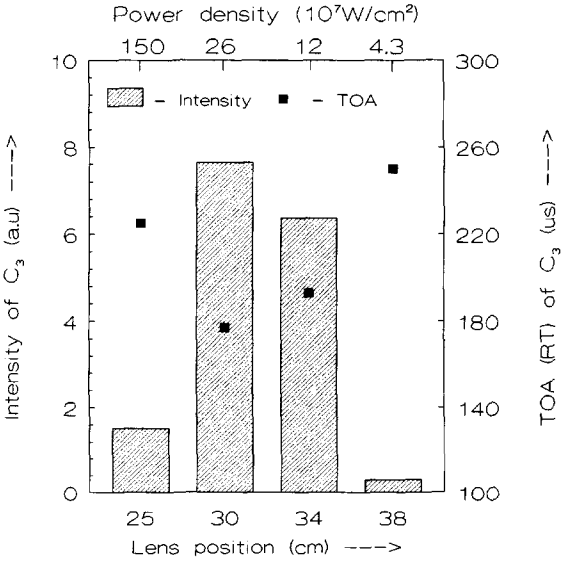

Fig. 4. Intensity and TOA data for C_3 as a function of laser power density.

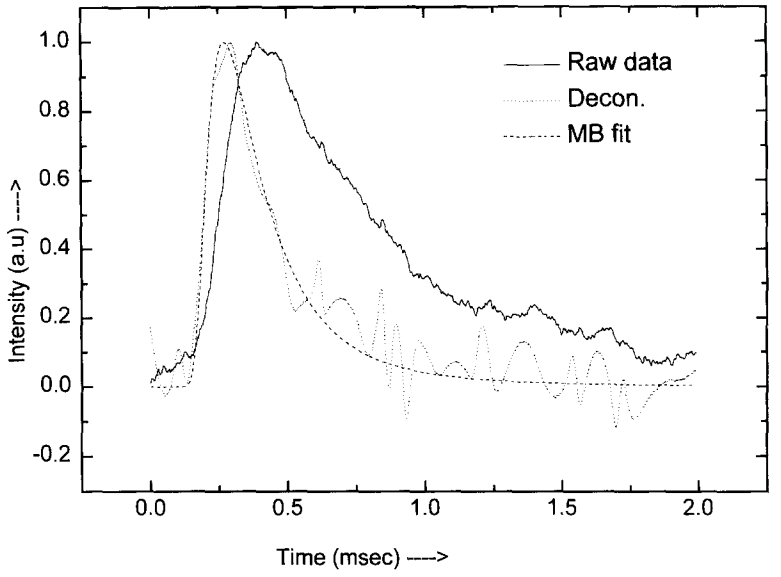

Fig. 5. TOA profile, deconvoluted and fitted Maxwell Boltzmann distribution curves for C_3 at a power density of 4.3×10^7 W/cm^2.

QMF detector at time t, A is a constant, m is the mass of the particle, z is the distance between the target and the detector, v_{gi} is the center-of-mass velocity, k is Boltzmann's constant and T is the temperature describing the stream velocity spread. The C_3 and UO molecules TOA profiles are well fitted by a sum of two distributions and the C_1^+ and UO^+ are well fitted by a single distribution. The parameters obtained from the fitting are shown in Table 1 and the fitted curves for the various species are shown in Figs. 5–9. It is apparent from the table of the fitted parameters for the TOA of C_3 and UO that there are two distributions; one with a high group velocity and lower temperature and the other with a low group velocity and higher temperature. The integrated areas of the two distributions differ from each other with in factor of three. We offer the following picture as an explanation for the observed distributions. During heating by a nanosecond laser pulse, the surface reaches its peak temperature nearly

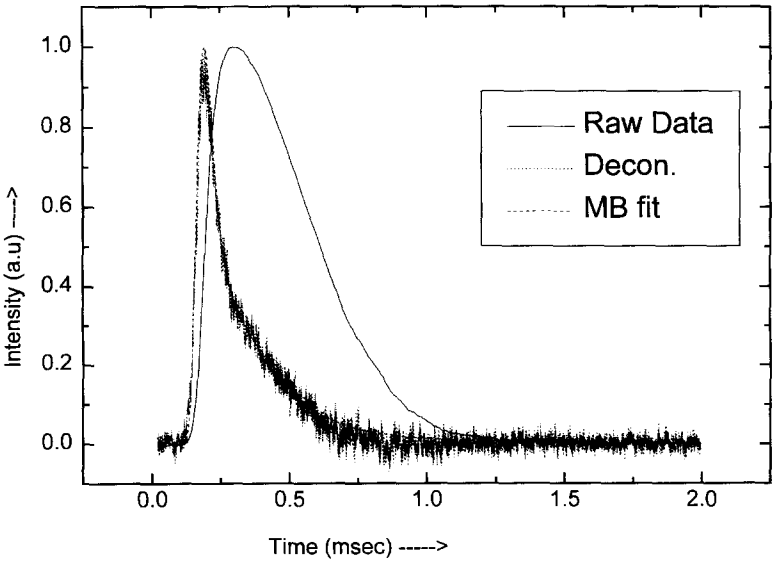

Fig. 6. TOA profile, deconvoluted and fitted Maxwell Boltzmann distribution curves for C_3, at a power density of 1.5×10^8 W/cm^2.

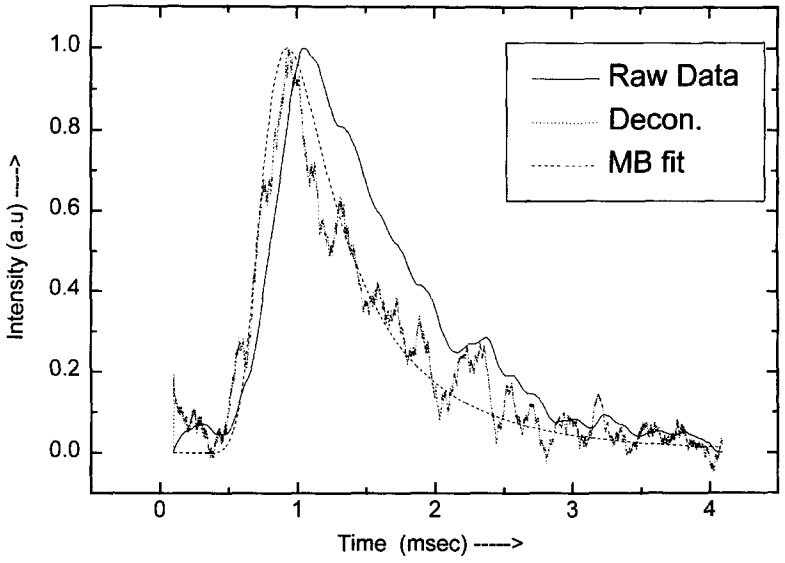

Fig. 7. TOA profile, deconvoluted and fitted Maxwell Boltzmann distribution curves for UO at a power density of 4.5×10^7 W/cm^2.

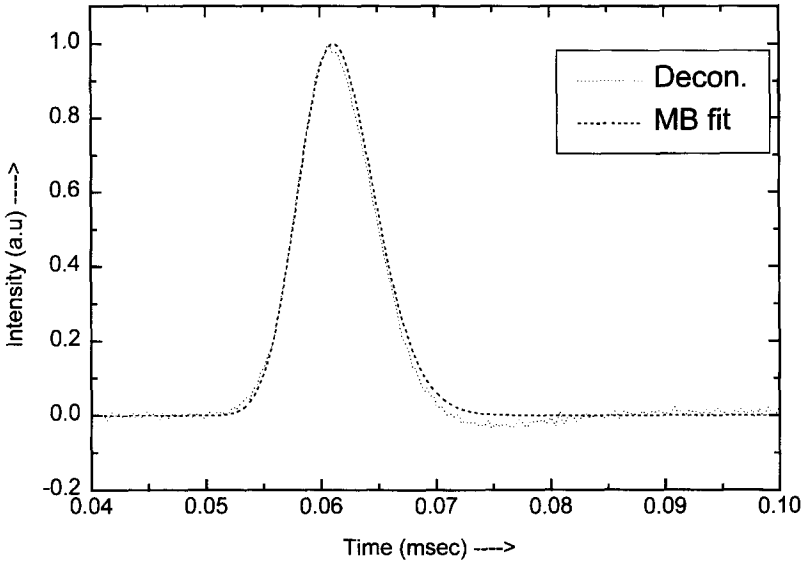

Fig. 8. Deconvoluted and fitted Maxwell Boltzmann distribution curves for C_1^+ at a power density of 1.5×10^9 W/cm^2.

Table 1
Parameters obtained by fitting the TOA profiles with shifted Maxwell Boltzmann distributions for various species at different densities

Species	Power density (10^7 W/cm^2)	v_{g1} (cm/s)	v_{g2} (cm/s)	$Temp_1$ (K)	$Temp_2$ (K)	$Area_1$ (a.u)	$Area_2$ (a.u)
C_3	4.3	5000	190000	2500	2000	1.706	1.637
C_3	12	30000	260000	3000	1200	3.445	2.637
C_3	26	45000	280000	3000	1200	4.4788	3.0733
C_3	150	45000	210000	3500	1500	5.3139	2.6907
C_1^+	150	–	905000	–	350	–	–
UO	4.5	0	50000	2500	600	3.8958	1.1946
UO	12	0	55000	2500	1750	3.9070	1.5076
UO^+	4.5	–	190000	–	50	–	–
UO^+	12	–	185000	–	50	–	–

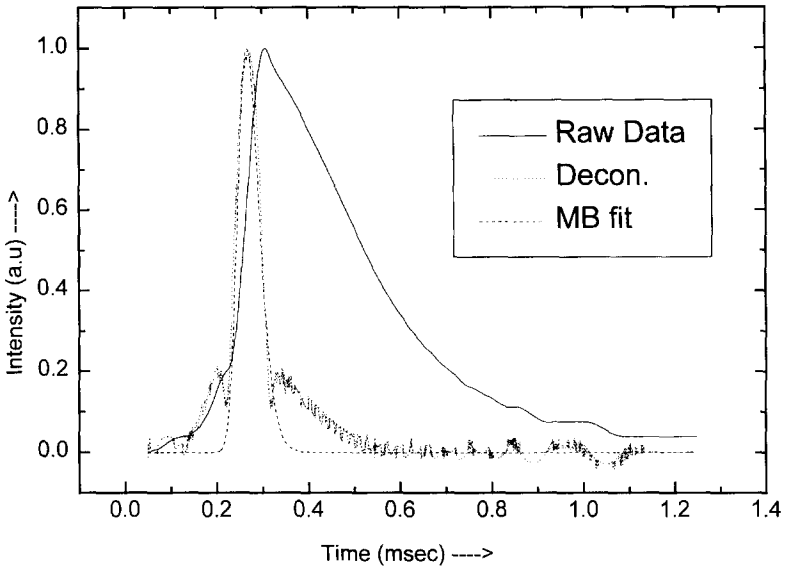

Fig. 9. TOA profile, deconvoluted and fitted Maxwell Boltzmann distribution curves for UO^+ at a power density of 1.2×10^8 W/cm^2.

at the end of the laser pulse and then begins to drop due to conduction and the energy required to evaporate with the evaporation rate corresponding to the surface temperature. In both these cases the temperature drops rather fast at initial times and the rate of decrease in temperature gets smaller at larger times. The net effect is that the sample spends less time around the peak temperature than it does at intermediate temperatures. At and around the peak surface temperatures the vaporization rate is large and the evaporation is followed by supersonic expansion because of the high density of molecules. The temperature describing the stream velocity spread becomes much smaller than the surface temperature but with a high group velocity [7]. The distribution with the high group velocity and lower temperature arises from the molecules evaporated at around the peak surface temperature followed by a supersonic expansion. The distribution with a low group velocity and higher temperature arises from the molecules evaporated at intermediate temperatures of the sample followed by effusion. Since the sample stays at intermediate temperatures for a much longer time than at and around peak surface temperature, the integrated areas of the two distributions are within a factor of three, even though the evaporation rates at intermediate temperatures are smaller. If the sample spends the same time at the intermediate temperatures as at and around the peak surface temperature then the contribution from the low group velocity distribution to the measured profile would have been negligible.

The C_1^+ and UO^+ TOA profiles are fitted by much larger group velocities and much lower temperatures compared to neutral species. The velocities of the ions are much larger than those expected from the estimated surface temperatures from the equation [8] as

$$T_s = (2E/K)(Dt/\pi)^{1/2},$$

where T_s, E, K, D and t are, respectively, the surface temperature, laser power density, thermal conductivity, thermal diffusivity and laser pulse width. The additional energy comes from the inverse bremsstrahlung absorption of the laser photons. We can estimate the extent of absorption from the absorption coefficient discussed by Singh and Narayan [9],

$$\alpha_p = 3.69 \times 10^8 \left(Z^3 n_i^2 / T^{0.5} \nu^3\right)\left[1 - \exp(-h\nu/kT)\right],$$

where Z, n_i and T are, respectively, the average charge, ion density and temperature of the plasma and h, k and ν are the Plank constant, Boltzmann constant and the frequency of the laser light, respectively. Based on this equation, it turns out that every single ion that evaporates from the surface absorbs a photon. There can also be acceleration of ions because of the space charge field present within a few Debye lengths from the surface. In the supersonic expansion the cooling depends on the effectiveness of the collisions in the energy redistribution. The low temperatures compared to the neutral species arise from the long range potentials of the ions during collisions in the supersonic expansion.

4. Conclusion

The plume generated by the laser evaporation of UO_2 and graphite targets were analyzed by a QMF. The time resolved spectrum was obtained for each of the observed vapour species. These TOA data are fitted by shifted Maxwell Boltzmann distributions and the translational temperatures and velocities obtained are reported. For neutral species, the deconvoluted TOA spectra are fitted well with the sum of two distributions, whereas for ions it

is fitted with one distribution. These results are explained with regard to the processes that happen in laser vaporization.

References

[1] R.W. Ohse, J.F. Babelot, C. Cercignani, P.R. Kinsman, K.A. Long, J. Magill, A. Scotti, in: Characterization of High Temperature Vapors and Gases, ed. J.W. Hastie, Proc. 10th Mater. Res Symp., NBS SP-561/1 (US Government Printing Office, Washington DC, 1979) p. 83.

[2] J.W. Hastie, D.W. Bonnell, P.K. Schenck, M. Joseph, in: Symposium on High Temperature Materials Chemistry, ed. W.B. Johnson and R.A. Rapp (Electrochemical Society, Pennington, 1990) p. 156.

[3] M. Joseph, N. Sivakumar, D. Darwin Albert Raj, C.K. Mathews, Rapid Commun. Mass Spectrosc. 10 (1996) 5.

[4] R.W. Ohse, J.F. Babelot, C. Cercignani, J.P. Hiernaut, M. Hoch, G.J. Hyland, J. Magill, J. Nucl. Mater. 130 (1985) 165.

[5] D.W. Bonnell, P.K. Schenck, J.W. Hastie, Int. Symp. Laser Process for Microelectronic Applications, 172nd Electrochemical Society Meeting, 1987.

[6] Q. Zhuang, K. Ishigoh, K. Tanaka, K. Kawano, R. Nakata, Jpn. J. Appl. Phys. 43 (1995) L248.

[7] C.-H. Tsai, D.R. Olander, Phys. Fluids 30 (1987) 386.

[8] R.S. Adrain, J. Watson, J. Phys. D17 (1984) 1915.

[9] R.K. Singh, J. Narayan, Phys. Rev. B41 (1990) 8843.